Fermilab

Fermi National Accelerator Laboratory
P.O. Box 500 • Batavia, Illinois • 60510

TD-98-010
February 5, 1998

HGQS03 End Field Analysis

G. Sabbi

1 Introduction

The main new feature of the HGQS03 coil configuration, as compared to the first two HGQ models, is the design of the joint connecting the inner and outer coil in the lead end of each quadrant. HGQS01 and HGQS02 feature an external splice [1] placed outside the radial boundary of the coil, therefore requiring the use of special end collets for mechanical support. HGQS03 features an internal splice [2] entirely contained within the radial boundary of the coil. The goal is to provide a better mechanical support and to simplify the magnet assembly by replacing the end collets with collars over the whole length. In this note, a magnetic field analysis of the new lead end configuration is presented. The return end configuration in HGQS03 is identical to that of HGQS02: its magnetic field analysis has been presented in [3].

2 Computer model

The four main conductor groups in HGQS03 have the same geometry as in HGQS02. They have been optimized using BEND [4]. The internal splice geometry, which has been optimized using LEAD, is shown in Figure 1. The z axis is directed outwards from the magnet body, and its origin is chosen following [1]. The lead conductor at the pole of the inner coil is ramped up to the outer coil radius starting at z=-137.83 mm. The ramp ends at z=-23.53 mm. From this point the conductor continues straight until z=0, then it is bent back 180 degrees towards the magnet body. In the outer coil, only a 180 degree turn is needed, which starts and ends at at z=0. The splice length is 137.83 mm. The iron yoke starts at z=-150 mm.

The magnetic field analysis has been performed using ROXIE [5]. The 3D model of the coil is built by extrusion along the z axis, starting from a 2D cross-section model shown in Figure 2. In each layer, the blocks and conductors are numbered from midplane to pole, starting with the outer layer. For the main conductor groups, the BEND coordinates files which specify the cross-sections of each conductor at 50 locations along z have been transferred to ROXIE using the BEND-ROXIE interface. These data are then interpolated to 30 new axial positions chosen according to the ROXIE algorithm. The geometry of the internal splice has been defined using the "additional bricks" feature in ROXIE. In order to simplify the input procedure, a small extension to ROXIE has been written, which allows the use of some symmetry operations on the additional bricks. The ROXIE block/conductor definitions and the BEND definitions for the corresponding conductor groups are reported in table 1. Figure 3 shows the resulting ROXIE model of the HGQS03 lead end. A straight section extending from the edge of the iron yoke for 1.5 m in the negative z direction is also included in the model.

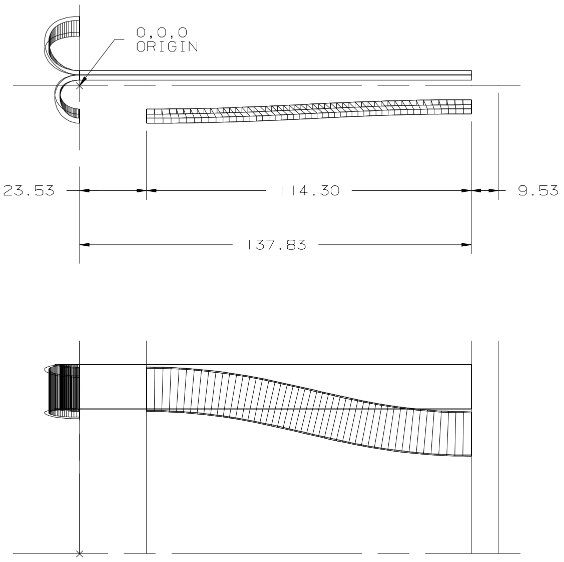

Figure 1: HGQ internal splice geometry [2].

Table 1: Block and turn definitions.

ROXIE				BEND	No. turns	Description
Blk	Turn	Conn. blk	End type	Group		
1	1		1		1	Straight to quadrant splice
2	2 to 15	4	2	q2ol311	14	2^{nd} wound, outer, left
3	16	5	3	q1or01	1	1^{st} wound, outer, left
4	17 to 30	2	7	q2ol212	1	2^{st} wound, outer, right
5	31	3	8	q1ol01	1	2^{st} wound, outer, right
6	32	10	12		1	Straight to coil spilce (outer)
7	33 to 42	12	4	q2il19	10	2^{nd} wound, inner, left
8	43	13	5	q1il01	1	2^{nd} wound, inner, left
9	44 to 45	13	6	q1il02	2	1^{st} wound, inner, left
10	46	6	13		1	Straight to coil splice (inner)
11	47		9		1	Straight to quadrant splice
12	48 to 57	7	10	q2il28	10	2^{nd} wound, inner, right
13	58 to 60	8,9	11	q1ir03	3	1^{st} wound, inner, right

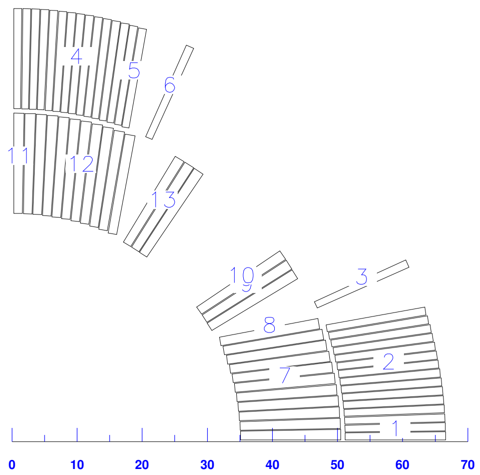

Figure 2: Coil cross-section model (first quadrant). Axis scale is in mm.

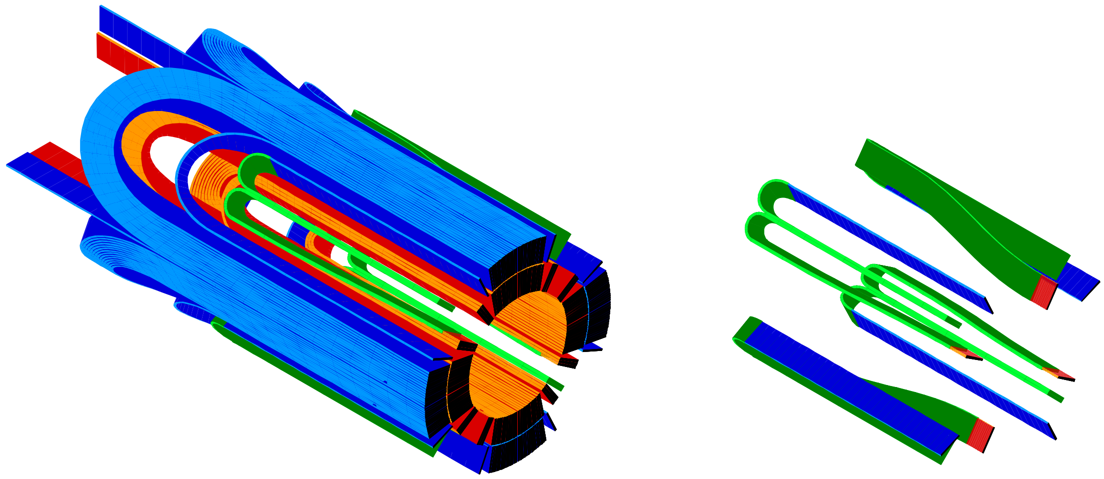

Figure 3: HGQS03 lead end model.

The field calculation is based on the Biot-Savart law. The iron yoke is regarded as a magnetic mirror of circular shape (inner radius 9.256 cm) with infinite permeability. For the ROXIE calculation, each conductor has been subdivided in current filaments, one for each strand. The total number of strands is 38 in the inner layer, 46 in the outer layer. For both the lead and the return end calculations, a straight section extending in the negative z direction for 1.5 m from the start of the iron yoke towards the magnet body is also included in the model.

3 Peak field

The 3D peak field is obtained by calculating the magnetic field on each strand at the longitudinal cuts which specify the geometry. Since the critical current density has been measured for a strand without compensation for the self field, the influence of the self field of each strand is neglected in the peak field calculation. The contribution of the iron yoke is not taken into account. However, previous calculations [6] show that the distance from the edge of the iron yoke to the coil end (150 mm) is sufficient to ensure that its contribution to the peak field can be neglected.

Outer Layer			Inner Layer		
Block #	Turn #	B^{max}/I T/kA	Block #	Turn #	B^{max}/I T/kA
1	1	0.420	7	42	0.608
2	15	0.571	8	43	0.602
3	16	0.534	9	45	0.629
4	30	0.544	10	46	0.639
5	31	0.544	12	57	0.609
6	32	0.534	13	60	0.639

Table 2: Field load line coefficients in the HGQS03 lead end.

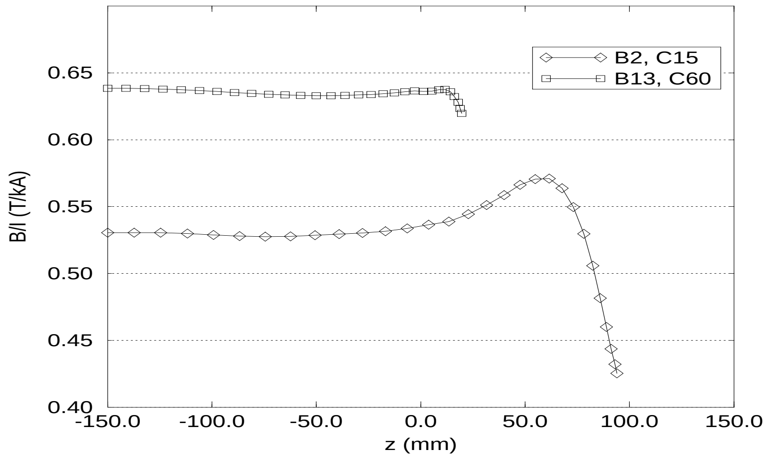

Figure 4: Field load line along z for the peak field conductors in the inner and outer layers.

The linear coefficients for the maximum field in each block of the lead end as function of current are reported in table 2. The load line coefficients for the maximum field in the magnet body at low current are 0.576 T/kA for the outer layer and 0.687 T/kA for the inner layer. Figure 4 shows the field load line along z for the peak field conductors in the inner and outer layers. They are not significantly different from those obtained for the external splice configuration [3]. Figure 5 shows the field load line along z in the lead conductors. The magnetic field decreases rapidly along the inner cable ramp. With respect to the respective peak field conductors in the lead end, the margin in the turnaround section of the splice is 0.033 T/kA for the outer cable, 0.102 T/kA for the inner cable. A low field is achieved in the splice area.

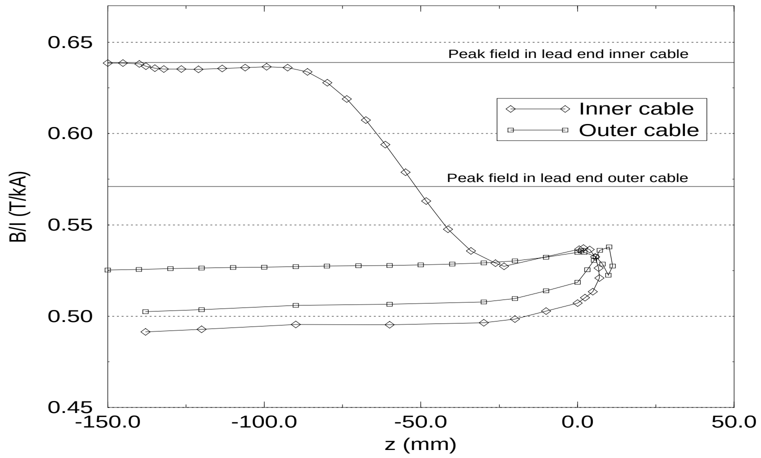

Figure 5: Field load line along z in coil splice conductors.

4 Field quality

The field quality in the end regions will be expressed in terms of integrated multipole components, defined according to the following expression:

$$\int_{z_p}^{z_q} [B_y(x,y,z) + iB_x(x,y,z)]dz = \sum_{n=1}^{\infty} (\hat{B}_n{}^{[z_p,z_q]} + i\hat{A}_n{}^{[z_p,z_q]}) \left(\frac{x+iy}{r_0}\right)^{n-1} \tag{1}$$

This expansion is only valid if the integration interval covers the whole end region, i.e. if the starting point z_p is sufficiently inside the magnet body and the end point z_q is sufficiently far away from the coil termination. In general, the expansion for the 3D field in the end regions would require additional terms (pseudo-multipoles). However, the pseudo-multipole components integrate to zero and can therefore be eliminated provided that the longitudinal field component vanishes at the boundaries of the integration interval [7].

As for the magnet straigth section, it is convenient to express the integrated multipole components $\hat{B}_n$, $\hat{A}_n$ in the end regions in "units" of 10^{-4} of the main integrated quadrupole field $\hat{B}_2^{[z_p,z_q]}$:

$$\hat{b}_n^{[z_p,z_q]} = \frac{\hat{B}_n^{[z_p,z_q]}}{\hat{B}_2^{[z_p,z_q]}} \cdot 10^4 \tag{2}$$

$$\hat{a}_n^{[z_p,z_q]} = \frac{\hat{A}_n^{[z_p,z_q]}}{\hat{B}_2^{[z_p,z_q]}} \cdot 10^4 \tag{3}$$

The magnetic length L_m of the interval $[z_p, z_q]$ is defined as the length which would provide an equivalent integrated quadrupole field in the magnet body:

$$L_m^{[z_p,z_q]} = \hat{B}_2^{[z_p,z_q]}/B_2 \tag{4}$$

B_2 is the quadrupole field component in the straight section. For the present study, the integrated multipoles have been obtained from 50 line integrals of the transverse field, calculated along lines parallel to the z-axis, at the reference radius of 1 cm and equally spaced azimuthal angles. The integration range is [-35,+25] cm. This ensures that the longitudinal component of the magnetic field at the boundaries of the integration intervals is negligibly small and that the field integral can be expanded according to equation 1. Each field integral has been evaluated by adding up the contributions calculated at 1 mm intervals along z. The magnetic length calculation is based on a transfer function in the magnet body of 18.22 T/m/kA, as obtained for a 2D analysis carried out under the same assumptions (conductors aligned to the coil outer radius, circular iron yoke of inner radius 9.2564 cm and infinite permeability) [8]. The results for the magnetic length and the average multipole components in the HGQS03 lead end are reported in table 3. The corresponding integrated multipoles for HGQS02 and HGQS01 are also reported for comparison: as can be seen, from the field quality standpoint, the new configuration is substantially equivalent to the previous ones. The integrated multipoles in the return end are identical to those of HGQS02 [3], and are reported in Table 4.

Table 3: Integrated harmonic coefficients in the HGQS03 lead end. The integration interval starts at z=-35 cm and ends at z=+25 cm. The corresponding values for HGQS02 and HGQS01 are reported for comparison [3, 10].

Parameter	HGQS03	HGQS02	HGQS01
L_m (cm)	41.54	41.39	40.72
$\hat{b}_2$	10000	10000	10000
$\hat{b}_6$	0.594	0.657	0.597
$\hat{b}_{10}$	-0.0033	-0.0032	-0.0032
$\hat{b}_{14}$	-0.000014	-0.000015	-0.000015
$\hat{a}_2$	43.82	38.54	42.8
$\hat{a}_6$	-0.041	0.020	0.025
$\hat{a}_{10}$	-0.0006	-0.0011	-0.0011
$\hat{a}_{14}$	0.000004	0.000007	0.000006

In order to analyze the contributions to the integrated harmonic components from different parts of the coil end, and to compare different configurations, it is convenient to split the integration in a sequence of short consecutive intervals along z: $[z_i, z_{i+1}], i = 1, N$, with $z_i = z_p + (i-1)\Delta$, $\Delta = (z_q - z_p)/N$. For this purpose, the integrated multipole componenents are most conveniently expressed in terms of "units" of 10^{-4} of the integral of the main quadrupole field B_2 *in the straight*

Parameter	HGQS03/HGQS02	HGQS01
L_m (cm)	32.50	31.78
$\hat{b}_2$	10000	10000
$\hat{b}_6$	0.140	0.048
$\hat{b}_{10}$	-0.0040	-0.0041
$\hat{b}_{14}$	-0.000017	-0.000017

Table 4: Integrated harmonic coefficients in the return end of HGQS03/HGQS02 [3], and corresponding values for HGQS01 [10]. The integration interval starts at $z = -25$ cm and ends at z=+25 cm.

section extended over the same physical length:

$$\bar{b}_n^{[z_i,z_{i+1}]} = \frac{1}{B_2\Delta}\hat{B}_n^{[z_i,z_{i+1}]} \cdot 10^4 \tag{5}$$

$$\bar{a}_n^{[z_i,z_{i+1}]} = \frac{1}{B_2\Delta}\hat{A}_n^{[z_i,z_{i+1}]} \cdot 10^4 \tag{6}$$

It should be noted that since the intervals $[z_i, z_{i+1}]$ do not in general satisfy the requirement of vanishing longitudinal field at their boundaries, the Fourier expansion 1 for the $\hat{B}_n^{[z_i,z_{i+1}]}$ components is only valid at the radius r_0. The relation between the $\bar{b}_n$, $\bar{a}_n$ components and the $\hat{b}_n$, $\hat{a}_n$ components is obtained as follows: from 1 and 5,

$$\hat{B}_n^{[z_p,z_q]} = \sum_{i=1}^{N} \hat{B}_n^{[z_i,z_{i+1}]} = B_2\Delta 10^{-4} \sum_{i=1}^{N} \bar{b}_n^{[z_i,z_{i+1}]} \tag{7}$$

At the same time, from 2 and 4,

$$\hat{B}_n^{[z_p,z_q]} = B_2 L_m 10^{-4} \hat{b}_n^{[z_p,z_q]} \tag{8}$$

Finally, from 7 and 8,

$$\hat{b}_n^{[z_p,z_q]} = \frac{\Delta}{L_m} \sum_{i=1}^{N} \bar{b}_n^{[z_i,z_{i+1}]} \tag{9}$$

The HGQS03 $\bar{b}_n$ and $\bar{a}_n$ components as function of z for the orders n=2, 6, 10 in the range [-35, +25] cm are reported in Figure 6 to 11. They have been calculated with Δ=2 mm, using 3 integration points in each interval. The corresponding values for HGQS02 are also reported for comparison.

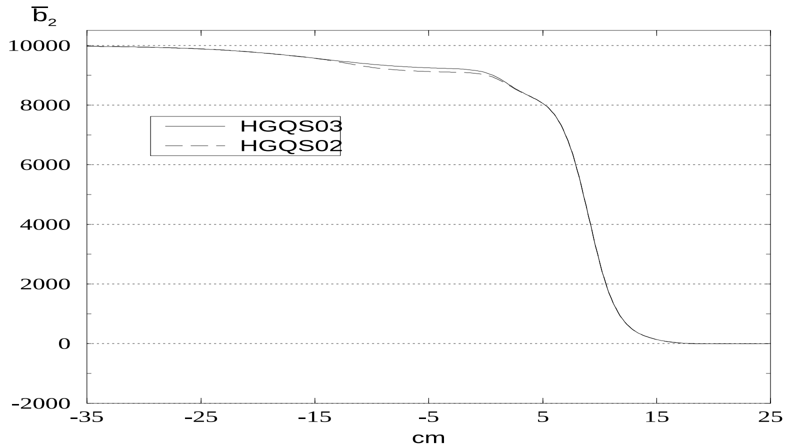

Figure 6: Contributions to the integrated normal quadrupole.

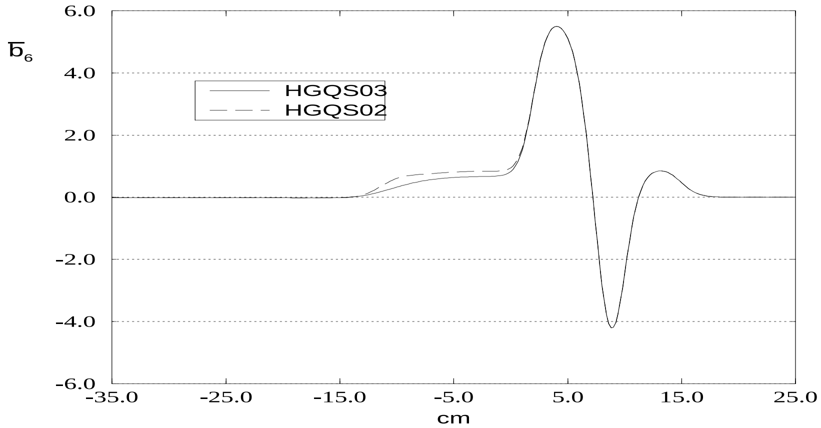

Figure 7: Contributions to the integrated normal dodecapole.

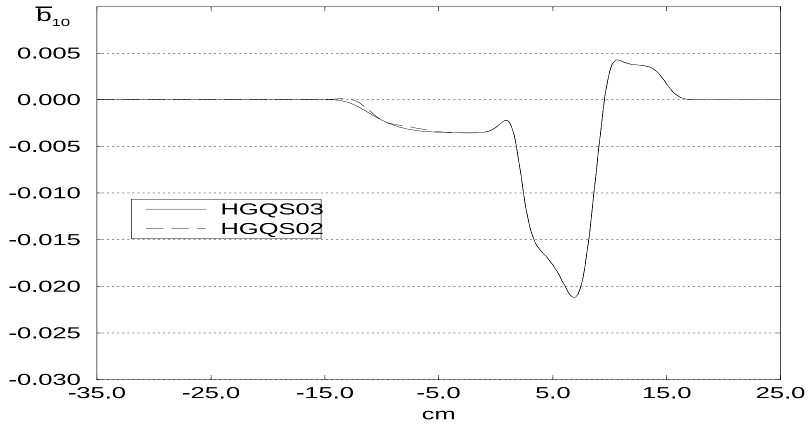

Figure 8: Contributions to the integrated normal 20-pole.

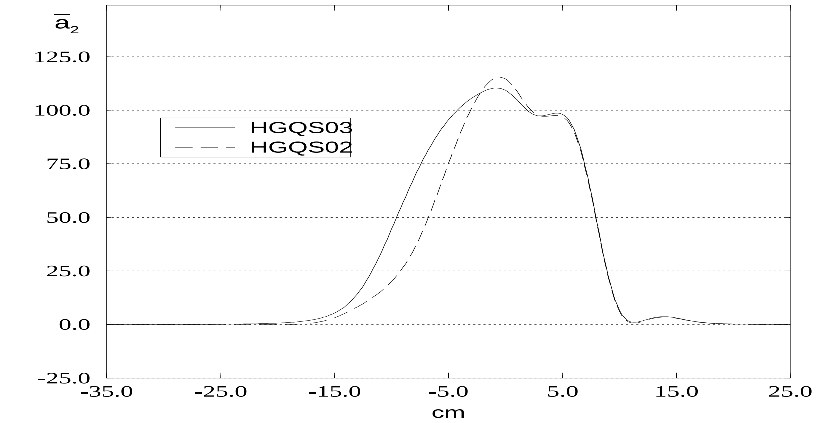

Figure 9: Contributions to the integrated skew quadrupole.

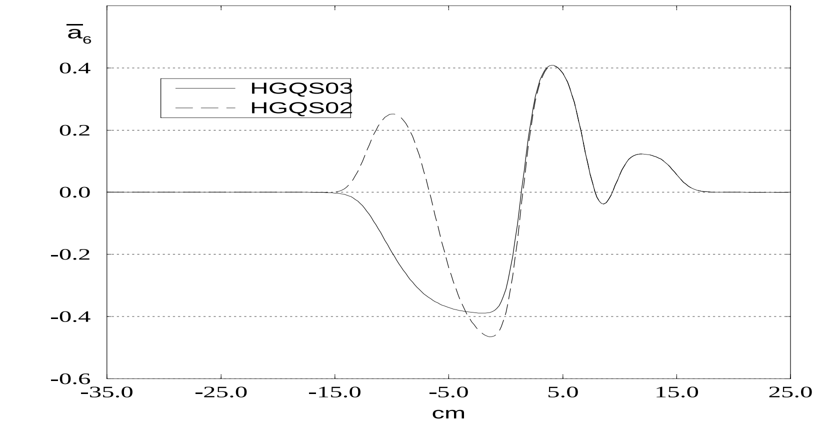

Figure 10: Contributions to the integrated skew dodecapole.

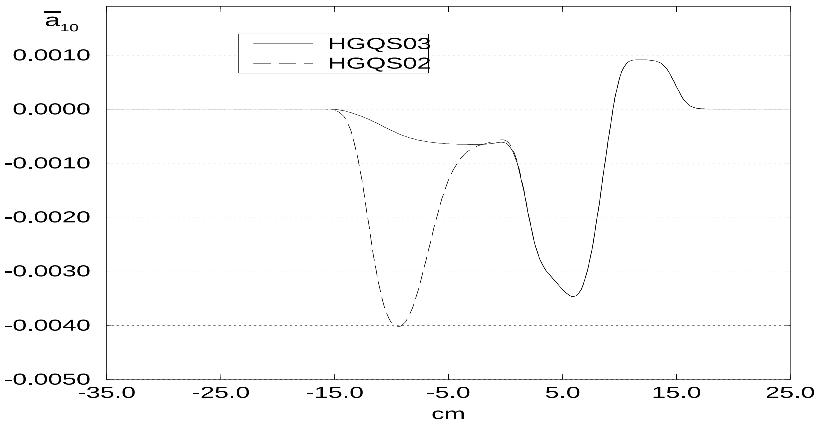

Figure 11: Contributions to the integrated skew 20-pole.

If the quantities $\bar{b}_n^{[z_i, z_{i+1}]}$ are regarded as continuous functions $\bar{b}_n(z)$, equation 9 can be rewritten as follows:

$$\hat{b}_n^{[z_p, z_q]} = \frac{1}{L_m} \int_{z_p}^{z_q} \bar{b}_n(z) dz \tag{10}$$

In order to carry out a beam tracking analysis where the local variation of the field is taken into account, a 3D expansion of the local (longitudinal and transverse) field in terms of pseudo-multipoles is needed. The expansion can be built starting from the field values $\vec{B}(r_0, \theta_i, z_j)$ calculated on a cylindrical surface inside the magnet bore [9]. These data have been calculated for $r_0 = 1$ cm, at 50 different angles and 1 mm axial spacing, and are available upon request.

5 Conclusions

A magnetic field analysis of the HGQS03 lead end, which features an internal coil to coil splice, has been presented. From the maximum field and field quality standpoint, the internal splice configuration is substantially equivalent to the external splice configuration in HGQS02. A good margin is obtained along the ramp and in the splice area.

References

[1] J. Brandt, A, Simmons, "Coil End Design for the LHC IR Quadrupole Magnet", Fermilab TS-96-013, November 1996.

[2] J. Brandt, "LHC IR Quad Internal Splice Design", March 10, 1997.

[3] G. Sabbi, "End Field Analysis of HGQ Model S02", Fermilab TD-97-045, October 1997.

[4] J. Cook, *"Strain Energy Minimization in SSC Magnet Winding"*, IEEE Transactions on Magnetics, vol. 27, pp. 1976-1980, March 1991.

[5] S. Russenschuck, "A computer program for the design of superconducting accelerator magnets", Proc. ACES Symposium, Monterey, California, 1995 and CERN AT/95-39, September 1995.

[6] S. Caspi, "LHC IR Quad", FNAL/LBL/CERN videoconference meeting, May 1st, 1996.

[7] S. Caspi, M. Help, L. Laslett, "3D Field Harmonics", LBL Report SC-MAG-328, March 1991.

[8] G. Sabbi, *"Load lines and short sample limits for HGQ model S01"*, Fermilab TD-97-011, April 1997.

[9] S. Caspi, M. Helm, L. Laslett, V. Brady, "An approach to 3D Magnetic Field Calculation Using Numerical and Differential Algebra Methods", LBL SC-MAG-395, July 1992.

[10] G. Sabbi, "Magnetic Field Analysis of HGQ Coil Ends", Fermilab TD-97-040, September 1997.